JOURNAL OF AIRCRAFT
Vol. 37, No. 2, March–April 2000

Evaluation of Computational Algorithms Suitable for Fluid-Structure Interactions

Marilyn J. Smith* and Dewey H. Hodges†
Georgia Institute of Technology, Atlanta, Georgia 30332-0150
and
Carlos E. S. Cesnik‡
Massachusetts Institute of Technology, Cambridge, Massachusetts 02139

The objective was to identify and mathematically evaluate suitable methods to transfer information between nonlinear computational fluid dynamics (CFD) and computational structural dynamics (CSD) grids. This data transfer is vital in the field of computational aeroelasticity, where the interpolation method between the two grids can easily be the limiting factor in the accuracy of an aeroelastic simulation. The data to be transferred can include a variety of field variables, such as deflections, loads, pressure, and temperature. For a method to be suitable, it is important that it provide a smooth, yet accurate transfer of data for a wide variety of functional forms that the data may represent. An extensive literature survey was completed that identified current algorithms in use, as well as other candidate algorithms from different implementations, such as mapping and CAD/CAM. The performance of the various methods was assessed on a number of analytical functions, followed by a series of applications that have been or are currently being studied using nonlinear CFD methods coupled with linear representations of the CSD equations (equivalent plate/shell mode shapes and influence coefficient matrices). Two methods, multiquadric-biharmonic and thin-plate spline, are shown to be the most robust, cost-effective, and accurate of all of the methods tested.

Introduction

NONLINEAR computational fluid dynamics (CFD) methodologies, in particular the methods solving the Euler and Navier–Stokes equations, have become relatively mature, so that utilization of these methodologies in more complex, interdisciplinary problems is an area of development for current and future applications. One of these interdisciplinary applications is computational aeroelasticity (CAE). Traditionally, CFD methods have been applied to rigid configurations. In flight, aircraft components rarely, if ever, behave as a rigid body. The flexibility of the structure has a direct impact on aircraft performance, maneuverability and flight controls, etc. Thus, the ability of CFD methods to capture this flexibility can improve the capability of the designers and analysts to understand the complex interaction of unsteady aerodynamics and structural dynamics. This understanding can ultimately lead to a reduction in production and development costs by identifying deficiencies during the design/analysis phase of development. Additionally, this capability can aid in the analysis of problems that develop in the field as the role of the aircraft is redefined and expanded.

There are three primary classes of high-level CAE methodologies. The first class of methodologies is known as a fully coupled analysis or unified fluid–structure interaction. These methods reformulate the governing equations so that both the fluid and structural equations are combined into one set of equations. These new governing equations are solved and integrated in time simultaneously. An example of this application is the research code developed by Guruswamy.[1] This class of methodologies is not yet available in production aeroelastic codes with high-order aerodynamic load prediction capabilities.

The remaining two classes of methodologies can benefit from the application of more accurate interface algorithms. The second class, and currently the most widely used, is a closely coupled aeroelastic analysis, examples of which include ENS3DAE,[2] ENSAERO,[3] and CFL3DAE.[4] The aerodynamic and structural dynamics modules remain independent in their solutions, and their interaction is limited to the passage of surface loads and surface deformation information after each CFD time step or iteration.

The third class of methodologies is the loosely coupled analysis. Here, CFD analyses are updated by structural deflections only after partial or full convergence. Thus, grid deflection updates are performed sparingly, usually 3–10 times per analysis.[5,6] These computations have primarily been accomplished using CFD code and external interpolation and loads calculation routines that are uncoupled.

For the last two (and far more common) types of aeroelastic methodologies that solve the structural and fluid equations separately, the grids in the CFD and computational structural dynamics (CSD) methodologies are unlikely to coincide. Thus, an interpolation method to interface between the grids must be employed. Although the transfer of deformation data between aerodynamic and structural grids seems at first to be trivial, this is far from the case. The primary difficulty lies in the basic differences between the nature of the methods. CFD analyses are concerned with the flowfield surrounding the surface exposed to the flow. For example, flow around a rigid airfoil is dependent only on the profile of the airfoil. The internal structure that forms the shape of the airfoil is immaterial. Thus, a CFD grid is very fine around the exterior of the airfoil, wherever the changes in the flowfield characteristics are expected to be a maximum. Conversely, CSD methods examine the airloads on the surface and how these loads affect the internal structure of the airfoil. The CSD grid lies both on the surface and within the interior of the airfoil and is oriented to the structural components. Thus, the CFD and CSD grids are not only different in grid density, but quite likely the transfer of data between the two grids requires both extrapolation and interpolation.

Early efforts in the development of CFD–CSD interpolation algorithms centered on the application of one-dimensional splines[7,8] for both one- and two-dimensional structural panels. Harder and Desmarais[9] in the 1970s developed a method of surface splines for plates known as the infinite-plate spline (IPS) method that eliminated the need for the known points to be located in a rectangular array. These surface splines are the basis of several of the interpolation

Received 5 January 1998; revision received 10 May 1999; accepted for publication 16 September 1999.

*Assistant Professor, School of Aerospace Engineering. Associate Fellow AIAA.
†Professor, School of Aerospace Engineering. Fellow AIAA.
‡Assistant Professor, Department of Aeronautics and Astronautics. Senior Member AIAA.

schemes used today in finite element methods of MSC/NASTRAN[10] and ASTROS,[11] as well as modal interpolation programs such as MPROC3D.[12]

Initial efforts are underway by Blair[13] to examine new ways of developing the structural model so that the problems encountered by the disjoint CFD and CSD grids are eliminated. This method formulates the structural grid using a continuous surface spline based on bicubic functions of the two local surface directional variables. This method preserves smoothness and slopes between the structural elements. The formulation is appropriate for shell, beam, or plate structures. However, much work remains to be done before this methodology can be applied to full aeroelastic computations.

The linear and surface splines in use today were developed for beam and plate models and are not suitable in many instances for applications to shell structures that are being analyzed in the current state-of-the-art aeroelastic codes. These methods may introduce oscillations, discontinuities, or poor accuracy in the surface deformations that may result in errors in the final solution. This is particularly true for wing leading and trailing edges and other regions of high curvature. A systematic method is necessary to examine existing interpolation schemes, assess their strengths and weaknesses, develop new or modified schemes, and assess their applicability for a wide range of problems. It is assumed that the interpolations take place on individual aircraft components, rather than the entire structure at once. This includes evaluation of moving parts such as flaps, ailerons, etc., separate from the primary lifting surface. Aeroelastic computations were not actually computed using each interpolation method. It is assumed that accuracy and smoothness of the interpolated data will preserve the aeroelastic calculation accuracy.

Approach

As part of the development of a generic interface method, the manner through which information is passed from the fluid regime to the structural regime was examined. A full review of appropriate algorithms was undertaken, and the top candidates were selected using the criteria of accuracy, smoothness, ease of use, robustness, and efficiency. These candidates were tested to examine their suitability for use in this application, and recommendations were formulated based on the results.

A literature search was performed to 1) identify or eliminate possible interpolation schemes based on previous research and 2) aid in and reduce the amount of investigation that must be done to determine the suitability of a potential scheme. This literature search encompassed not only methods applied to CFD–CSD interpolation, but also to other engineering disciplines as well as mathematical or scientific (physics, etc.) applications. An excellent review of these methods was given by Franke.[14]

The selection of candidate algorithms was made on the basis of the results of the literature search, as well as the experience of the investigators. Six selections were made: infinite plate splines (IPS), finite-plate splines, thin-plate splines, multiquadric-biharmonic, inverse isoparametric mapping, and nonuniform B-splines. The last method is used in many CAD/CAM applications.

Analytical tests were then performed to examine the behavior of the functions in situations that may be encountered in applications and that isolate specific behaviors, such as smoothness and extrapolation. By means of these tests, the functions were analyzed for their characteristics in two- and three-dimensional applications. Because these functions must provide both interpolation and extrapolation, the characteristics of their behavior and limits of operation were examined. Additionally, the algorithm's behavior was assessed for both flat and highly curved contours. Based on these results, the methods were applied to realistic applications to determine the accuracy of the interpolation and, if applicable, extrapolation for aeroelastic applications for use in Euler/Navier–Stokes-based methods.

Algorithm Descriptions

Full technical descriptions of each method are contained in Ref. 15. A short summary of each technique presented in this paper is included herein. Additional information on the inverse isoparametric method (IIM) and finite plate spline (FPS) method, which were not applied on these configurations, can be found in Ref. 15.

Infinite-Plate Splines (IPS)

The method of infinite-plate splines[9] is one of the most popular methods of interpolation, currently used in programs such as ASTROS and MSC/NASTRAN. This method is based on a superposition of the solutions for the partial differential equation of equilibrium for an infinite-plate. We first consider a set of N discrete grid points lying within a two-dimensional domain with Cartesian coordinates x_1 and x_2. Each grid point has associated with it a deflection H that defines the vertical position coordinate of the surface on which both structural and aerodynamic grid points are presumed to lie. For a one-dimensional problem, this equation is

$$H(x) = \sum_{i=1}^{N} \left[A_i + B_i(x - x_i)^2 + F_i(x - x_i)^2 \ln(x - x_i)^2 \right] \quad (1)$$

where $H(x)$ is the deflection, A_i, B_i, and F_i are undetermined coefficients, and x_i is the surface location of the known function.

Using solutions of the infinite-plate equation, one calculates the values of a set of concentrated loads, all presumed to act at the known data points that give rise to the required deflections. Those concentrated forces are then substituted back into the solution, thus providing a smooth surface that passes through the data. Thus, given the deflections of the structural grid points it is possible to interpolate to a set of aerodynamic grid points that, in general, do not coincide with the structural ones.

Some advantages to this method are that the grid is not restricted to a rectangular array and that the interpolated function is differentiable everywhere. Points far away from known points are extrapolated nearly linearly. A minimum of three points is required because three points are necessary to define a plane.

Multiquadric-Biharmonic (MQ)

The multiquadrics (MQ) method is an interpolation technique that represents an irregular surface. More recently named the multiquadric-biharmonic (also refered to here as MQ) method, it was used to perform interpolation of various topographies.[16] The original name reflects the method's use of quadratic basis functions; note that a quadric surface is one whose geometry is described by quadratic equations. The quadric surface used in most cases is a hyperboloid of revolution in two sheets. The addition of biharmonic to the name is due to an important proof that the equations governing the method can always be solved.[14] The interpolation equation investigated is

$$H(x) = \sum_{i=1}^{N} \alpha_i \left[(x - x_i)^2 + r^2 \right]^{\frac{1}{2}} \quad (2)$$

The MQ method is stable and consistent with respect to the user-defined parameter r that controls the shape of the basis functions. A large r gives a flat sheetlike function, whereas a small r gives a narrow conelike function. For nonzero values of r, MQ produces an infinitely differentiable function that preserves monotonicity and convexity. Later development and implementation by Kansa[17] and by the authors[15] show that the method's conditioning, accuracy, and general numerical performance are improved by 1) permitting r to vary among the basis functions, 2) scaling and/or rotating the independent variables for some applications where the magnitudes of the variables differ widely, and 3) applying it in overlapping subdomains.

Thin-Plate Splines (TPS)

Thin-plate splines (TPS, or surface splines) provide a means to characterize an irregular surface by using functions that minimize an energy functional.[18] This methodology is very similar to the MQ method. The primary difference in these two methods is the function solved. A one-dimensional version of the function is

$$H(x) = \sum_{i=1}^{N} \alpha_i |x - x_i|^2 \log |x - x_i| \quad (3)$$

Here, the problem is approached from an engineering or physical representation of the surface. That is, for a one-dimensional problem, elementary cubic splines can be interpreted as equilibrium positions of a beam undergoing bending deformation. For a two-dimensional problem (such as a surface), these splines can be determined from the minimization of the bending energy (thus defining the equilibrium position) of a thin plate (which reduces to IPS). Because these types of splines are invariant with rotation and translation, they are very powerful tools for the interpolation of moving or flexible surfaces. This method is not limited to two-dimensional problems, but is extendible to three-dimensional problems.

Nonuniform B-Splines (NUBS)

The nonuniform B-splines (NUBS) method is based on the fact that splines in their most primitive form are used to represent curves in three-dimensional space. Therefore, a tensor product of two splines can be used to represent a surface in three-dimensional space. According to Ref. 19, to do the surface blending needed in aeroelastic applications, it is recommended that polynomial B-splines be used because rational splines have a tendency to generate poles and cause numerical problems. The resulting method, therefore, represents a surface by the tensor product of two B-splines:

$$S_{kt}(x, y) = \sum_{i=1}^{m-1} \sum_{j=1}^{n-1} P_{ij} B_{ik}(x) B_{jt}(y) \tag{4}$$

where S is the surface deflection at any point (x, y), P_{ij} are coefficients multiplying these splines to fit the data (control points), and B_{ik} and B_{jt} are the B-splines in the x and y directions, respectively.

The NUBS method is implemented with the aid of a library of routines called DT_NURBS developed at the David Taylor Research Center.[19] Because these routines were originally developed for CAD usage, a main program and surface generating routine were written to implement the DT_NURBS package.

Limitations of Each Method

Some of the methods have intrinsic limitations based on their current formulation. These limitations are summarized in Table 1.

Computational Characteristics of Each Method

Based on sample analytical interpolations of data on a flat plate, the average computational time and memory of the schemes are ranked in Table 2. Significant CPU time reductions are possible, depending on the scheme chosen. In addition, several of the schemes required significantly less computational memory than other schemes.

Table 1 Limitations of the interface methods based on mathematical formulation

Method	Limitation
IPS	Minimum of three data (grid) points is necessary to describe the plane. Noncoincident points are required. Extrapolations are performed linearly.
MQ	No minimum of data (grid) points is required mathematically, but for accuracy at least three points to describe the plane should be used.
TPS	No minimum of data (grid) points is required mathematically, but for accuracy at least three points to describe the plane should be used.
FPS	Two-dimensional application of this method was only attempted in this research. Three-dimensional extension is possible.
NUBS	There must be four curves and four data points. Points cannot be coincident. Degenerate data without C^0 continuity is smoothed over. C^0 continuity is enforced.
IIM	Valid for two-dimensional interpolations only. No extrapolation is possible.

Table 2 Comparative rankings of the computational requirements for each scheme

Method	Relative CPU time	Relative CPU memory
IPS	1.0	1.0
FPS	0.93	1.125
MQ	0.024	0.206
TPS	0.019	0.206
NUBS	0.024	0.094
IIM	0.031	0.0281

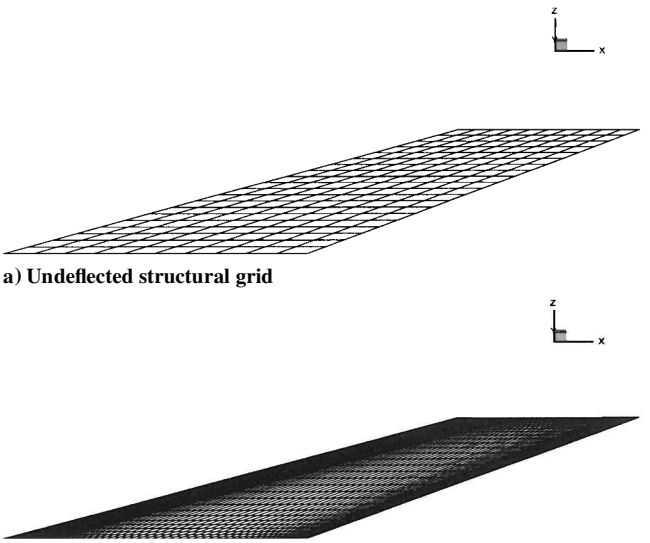

a) Undeflected structural grid

b) Undeflected aerodynamic grid

Fig. 1 AGARD 445 wing.

Representative Applications

This section describes the results of the applications test cases. It was not possible to test every algorithm discussed in Ref. 15 to each applications test case due to the nature of the algorithm implementation or due to limitations on the computational workstations used in this study. In the examples shown, graphical representations of the primary observations are presented as figures. Because of the space limitation, the reader is referred to Ref. 15 for a more complete discussion.

AGARD 445 Wing

The first test case examined is the interpolation of five modes of the AGARD 445 wing.[20] This test case represents a lifting surface, one of the most typical configurations analyzed by aeroelastic methods. The wing structure is represented by a flat plate that extends from the wing leading to trailing edges and from the wing root to the wing tip. This case involves pure interpolation with no extrapolation. The wing is a lifting surface whose motion is dominated by the motion in the z (Cartesian) coordinate. The x and y Cartesian coordinate motions are neglected.

In this test case, the structural grid is a regularly spaced mesh, 11 nodes in the streamwise direction and 31 nodes in the spanwise direction, shown in Fig. 1a. The aerodynamic grid encloses the actual wing surface, and comprises of 219 streamwise (110 on upper and lower surfaces) and 21 spanwise nodes. The grid is clustered at the leading and trailing edges, as seen in Fig. 1b. In these Figs. 1a and 1b, the view is a perspective of the wing that correlates with the mode deflection plots. The geometry of the wing is from left to right (leading to trailing edge) and from bottom to top (root to tip). Only the fifth mode that was interpolated is shown here in Fig. 2. Figure 2a is the contour of the modes, where each major increment

Table 3 Comparison of maximum deflections for the AGARD 445 wing modes

Mode	Original	IPS	NUBS	TPS	MQ
1	2.240	2.240	2.240	2.240	2.240
2	3.597	3.597	3.597	3.597	3.597
3	2.477	2.453	2.470	2.462	2.424
4	5.774	5.774	5.774	5.774	5.774
5	3.762	3.762	3.762	3.762	3.762

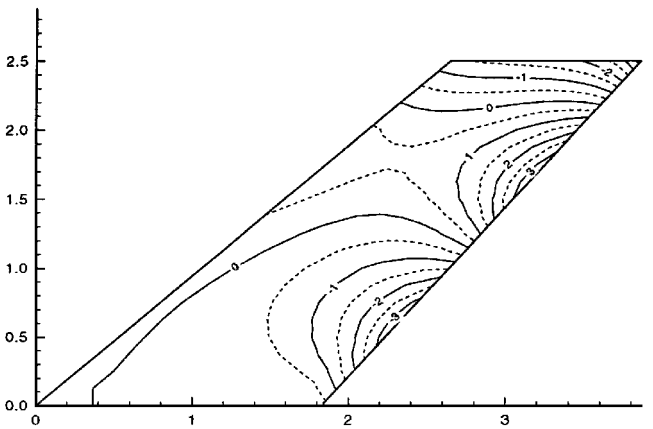

a) Structural grid (original) contours

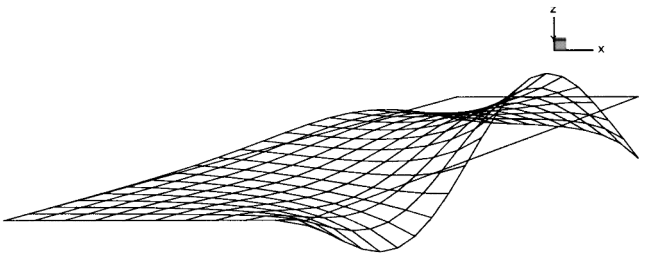

b) Structural grid (original) deflection

Fig. 2 AGARD 445 wing mode 5 plotted on the original structural grid.

of deflection is delineated with a solid line, with minor contours as dashed lines. Figure 2b has the mode (times a unit increment) superimposed on the surface to demonstrate the unit deflection of the surface. To provide a good visual perspective, the z Cartesian coordinate (direction of the deflections) has been expanded with respect to the wing planform. The wing root lies along the abscissa of each plot, with the leading edge located at 0.0 and the trailing edge at 1.8. The ordinate axis is the spanwise coordinate, with wing root at 0.0 and the wing tip at 2.5. The undeflected wing is outlined by the surface boundaries and is shown in perspective at the same scale as the deflections.

The AGARD 445 wing modes were interpolated using the IPS, MQ, TPS, and NUBS methods. The results of these methods for mode 5 are given in Figs. 3–6. The format of these plots follow the format of Fig. 2.

The primary difference in the prescribed modes and the interpolated modes is the outboard shift of the zero deflection point from the actual root line. This shift is characterized by the zero contour line at the root for most of the modes. Rather than blending smoothly at the root, the zero contour line has a tendency to turn parallel to the root chord. This may have a negative impact on the interface of a wing and a rigid fuselage. A comparison of the mode deflections shows that shifts in the contour lines for all modes and all methods were less than 2% of the chord. A comparison of the structural and interpolated aerodynamic maximum deflections is shown in Table 3, where the differences are minimal, the largest error less than 1% of the maximum deflection.

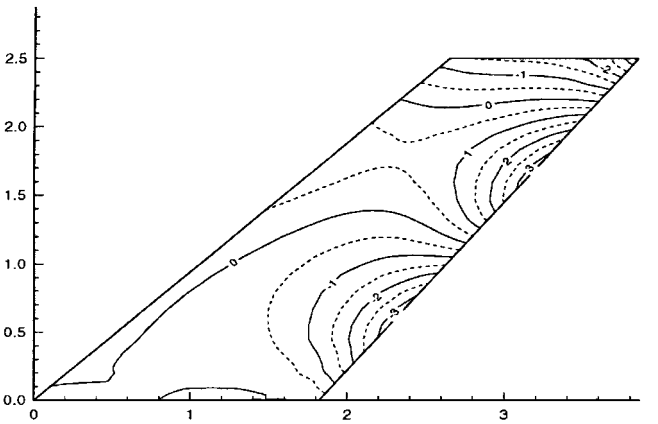

Mode contours

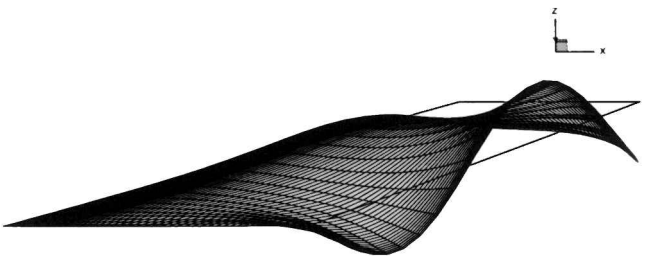

Mode deflection

Fig. 3 IPS results for AGARD 445 wing, mode 5.

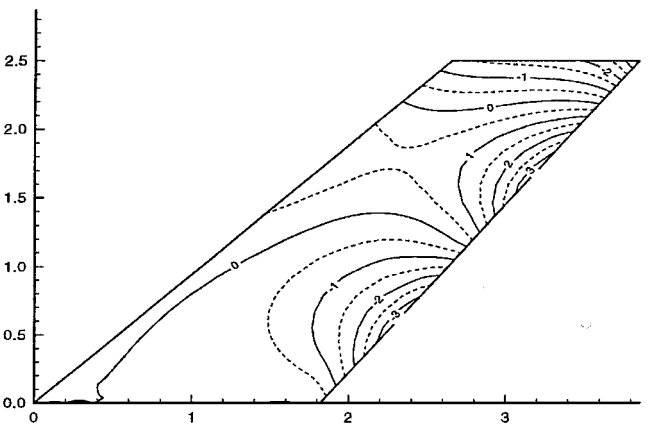

Mode contours

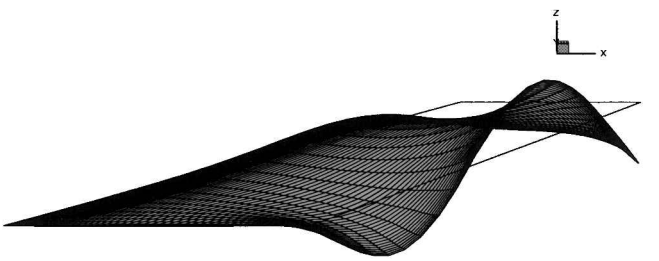

Mode deflection

Fig. 4 MQ results for AGARD 445 wing, mode 5.

Some oscillations are also noticeable in the interpolations, particularly near the edges (see also modes 4 and 5, Ref. 15). The IPS and NUBS methods have the most obvious oscillations, whereas the TPS method provides the most smooth and accurate representation. This discrepancy is very interesting to note because the IPS and TPS methods are based on the same derivation. The different implementation of the schemes may be partially responsible for this. Therefore, the implementation of the scheme plays an important role in the accuracy.

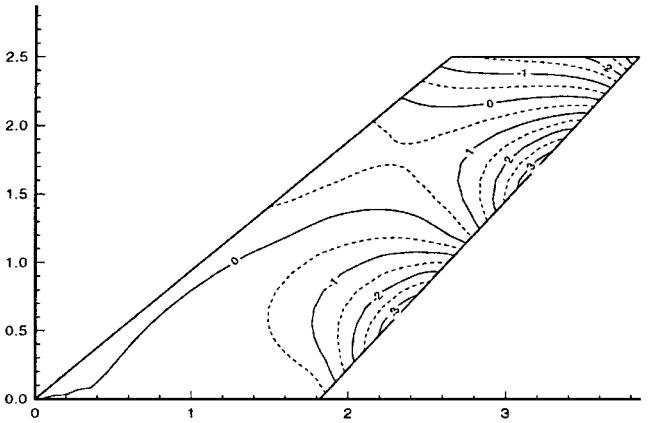

Mode contours

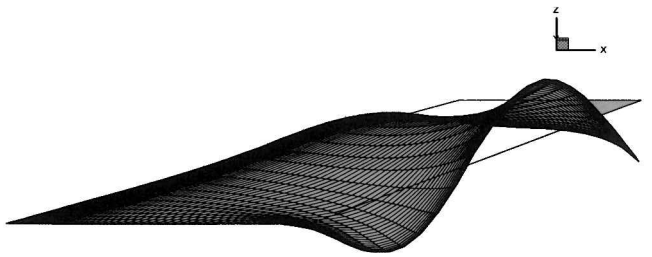

Mode deflection

Fig. 5 TPS method results for AGARD 445 wing, mode 5.

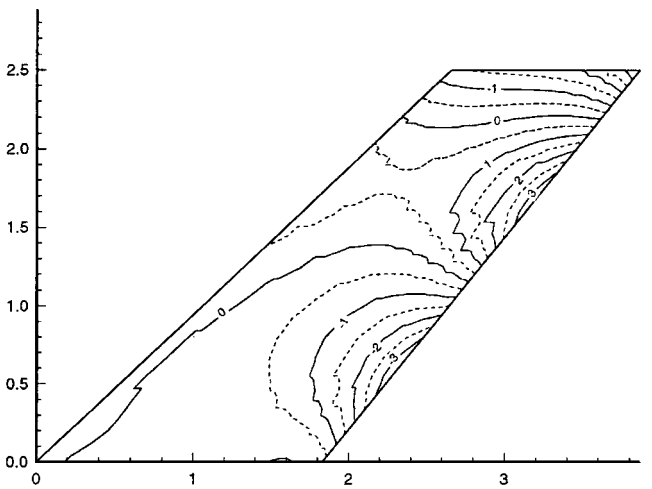

Mode contours

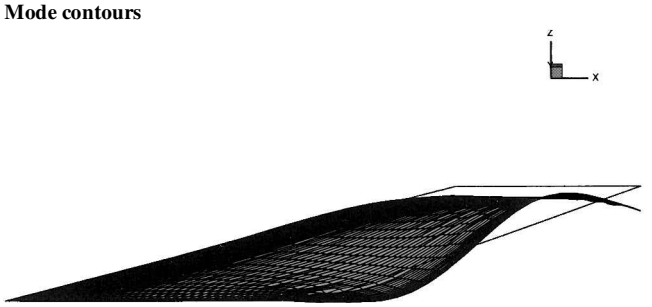

Mode deflection

Fig. 6 NUBS results for AGARD 445 wing, mode 5.

Engine Liner

The engine liner test case is an application the importance of which is growing as the problems of fatigue and aging aircraft increasingly become an issue. This particular case is based on an experimental effort[21] to determine the cause of flutter in an engine liner. A hostile aerodynamic environment surrounds the engine liner. The inner flow of the liner is usually very fast (near transonic speeds) and comprises the high-temperature exhaust core flow from the engine.

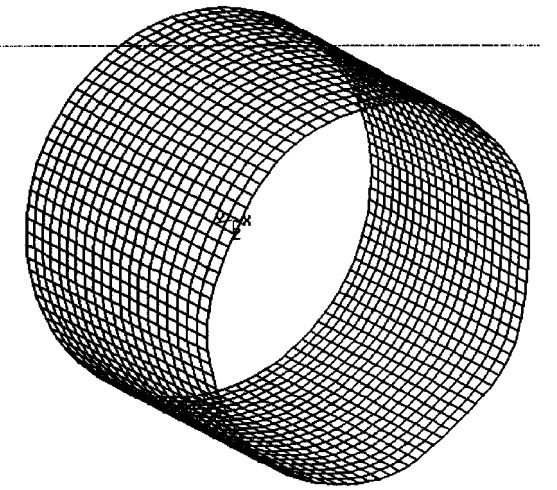

a) Structural grid

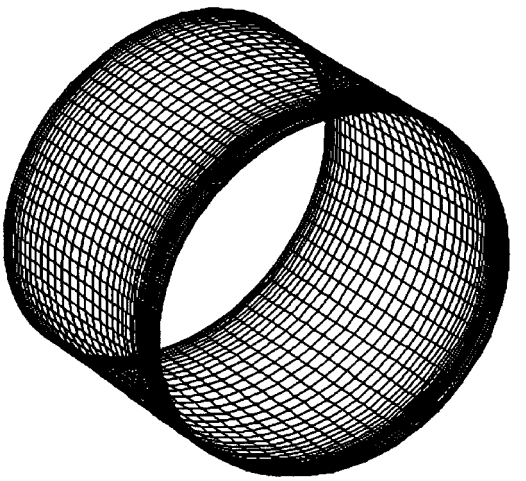

b) Aerodynamic grid

Fig. 7 Engine liner applications test case.

The outer side of the liner usually has ambient or bleed air flowing over it at different Mach and Reynolds numbers than the core flow. In addition, the liner dampers can trigger vortices. (Note that the liner dampers were not modeled during either the experimental or computational analyses.) A structural model was developed for the liner based on a series of small, interconnecting panels. The structural grid is shown in Fig. 7a. It comprised 97 nodes in the circumferential direction and 21 nodes in the streamwise direction. The aerodynamic surface grid, shown in Fig. 7b, was algebraically computed. This surface has 75 nodes in the circumferential direction and 45 nodes in the streamwise direction, clustered at the leading and trailing edges of the panel. As in the AGARD 445 wing test case, this test case involves pure interpolation, but includes all three Cartesian coordinate directions of motion.

The first five modes were deemed to be the primary influence in the motion of the liner. Here the fifth mode plotted on the structural mesh is shown as a typical example in Fig. 8. Notice that the leading edge of the liner is clamped (no deflections), whereas the trailing edge of the liner is permitted to move freely. The view for these figures is from the trailing edge of the liner looking forward. The liner forms a slight cone with the smaller radius located at the trailing edge. The use of contours is not appropriate due to the nature of the configuration. The asymmetry of the structure, superimposed with the modes, makes it impossible to view contours along the entire liner surface. The engine liner modes were interpolated using the IPS, TPS, and MQ methods. The remaining methods failed or were not suited (due to their limitations) for this particular configuration.

The results of the interpolations using these methods are given in Fig. 9. The IPS method did not work efficiently for the engine liner

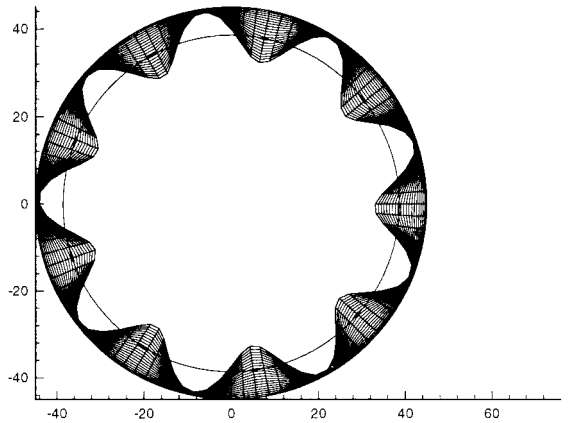

Fig. 8 Engine liner mode 5 plotted on original structural grid.

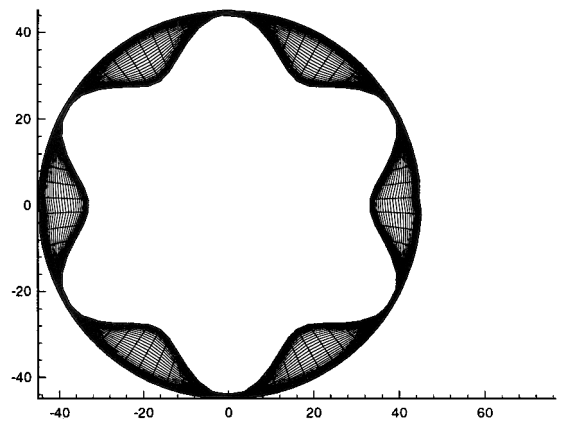

a) IPS method

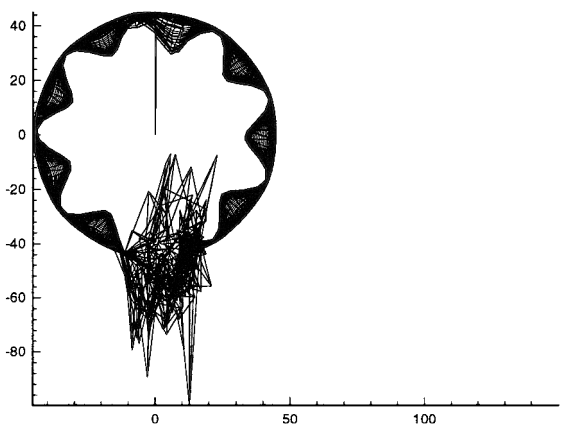

b) MQ method

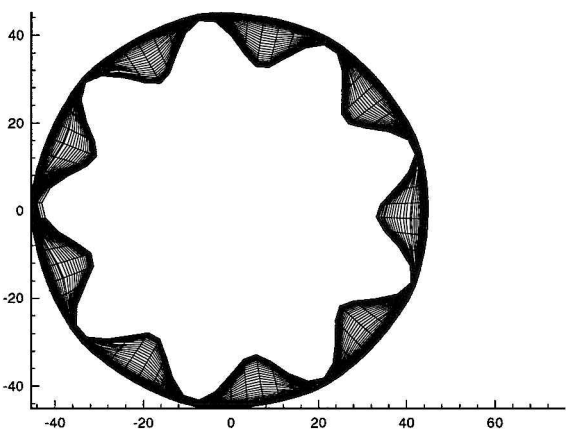

c) Scaled TPS method

Fig. 9 Engine liner mode 5 interpolation results.

Table 4 Comparison of maximum deflections for the engine liner modes[a]

Mode	Original	TPS (Unscaled)	TPS (Scaled)	MQ
1	5.737	123.1	5.713	131.8
2	5.801	82.75	5.775	27.06
3	5.797	197.0	5.770	84.25
4	5.611	28.03	5.670	14.54
5	5.676	26.65	5.653	157.3

[a]IPS values were not available.

Table 5 Structural and CFD meshes for the generic hypersonic vehicle

Component	Structural ($i \times j$)	CFD ($i \times j$)
Full fuselage	9×21	109×51
Split fuselage, upper	——	109×23
Split fuselage, lower	——	109×29
Upper wing	7×6	53×21
Lower wing	7×6	53×21

configuration due to the presence of multivalue points in the symmetry of the configuration. It was necessary to divide the liner into four separate configurations, run them separately, and then recombine the results to form the full configuration. Each section required approximately 30 min of workstation CPU time to complete (MQ and TPS required less than 5 min for the entire liner). If half of the liner or the full liner is run, IPS eventually fails with matrix solution errors after 1 h or more. As seen in mode 5, the interpolation appears to be excellent, with the exception of the break points in the liner. The mis-matching breakpoints mean that the integrity of the endpoints of the configuration is not maintained, as seen at the top of Fig. 9a.

It is evident that MQ has some problems with the engine liner. In Fig. 9b, the superimposed modes have very irregular oscillations at the top and bottom of the engine liner. When the MQ method is scaled or run using different r values, the problem shifts slightly but does not go away. The interpolation by TPS shows excellent results if the method is scaled. The mode deflections match almost identically in location and magnitude (within 1%) to the original data. For the unscaled run, TPS has problems similar to those encountered with the MQ method.

Table 4 shows a comparison of the magnitudes of the original and interpolated mode shapes. It is clearly seen that this test case poses a more rigorous test of the schemes' capabilities. The scaled TPS method gives results within 0.5% of the original data; but unscaled, the method yields an error that varies from 400 to 2000%. The MQ method provides results similar to the unscaled TPS method.

Lifting-Body Configuration

Another type of application test case is the lifting body. This type of vehicle is becoming ever more popular as new air/space vehicles are developed. Examples of these types of vehicles are the Space Shuttle, intercontinental ballistic missiles, and hypersonic vehicles. A generic lifting body with wings[22] was examined. This vehicle consists of separate upper and lower wing components, as well as a fuselage that is separated along the wing waterline, all of which are flexible and modeled with shell elements. This type of configuration is typical of H–H grids used in many current CFD methodologies. This configuration provided an opportunity to observe how well the methods performed on partial surfaces. (For example, the leading and trailing edges of the wing should match identically.) The different components of the vehicle are shown in Figs. 10 and 11 for the structural mesh and the CFD grid, respectively. The two meshes compare as shown in Table 5. There were a total of seven dominant modes for this model, the seventh of which is shown in Fig. 12, scaled to facilitate visualization.

The vehicle modes were interpolated using the MQ, IPS, and TPS methods. The results of each are shown in Figs. 13–15, respectively.

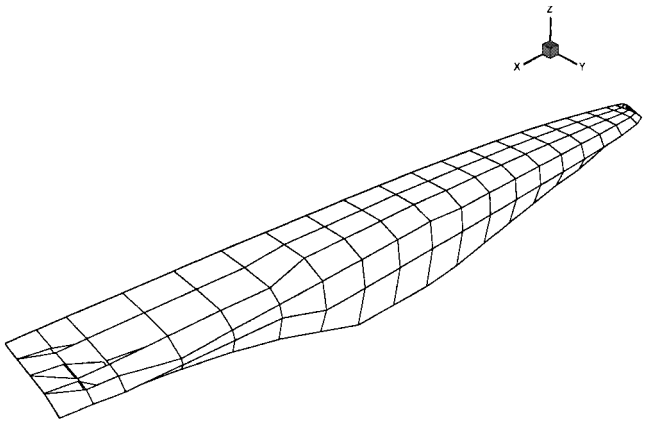

Fuselage grid

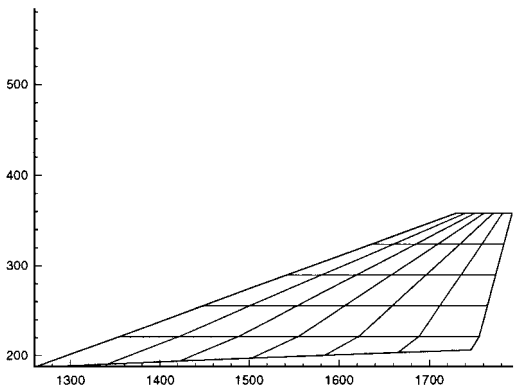

Wing grid

Fig. 10 Generic hypersonic vehicle structural grid.

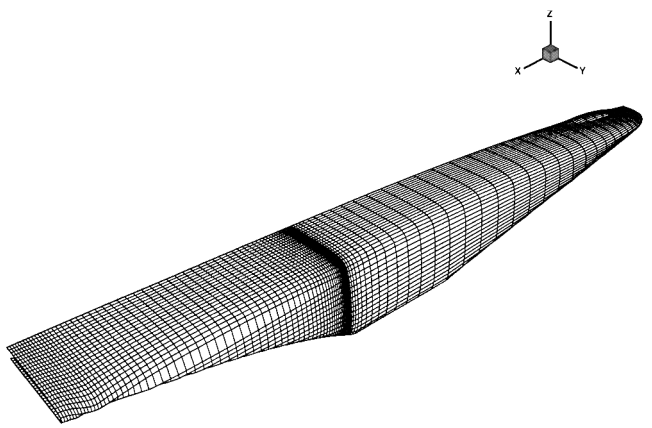

Fuselage grid

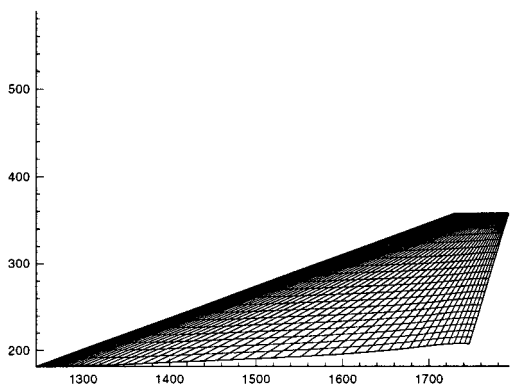

Wing grid

Fig. 11 Generic hypersonic vehicle aerodynamic grid.

Table 6 Comparison of maximum deflections for the generic hypersonic mode 1

Component	Original	IPS	TPS (scaled and unscaled)	MQ (scaled and unscaled)
Fuselage	1.405	1.414	1.415	1.411
Upper wing	1.490	1.579	1.491	1.570
Lower wing	1.490	1.580	1.491	1.569

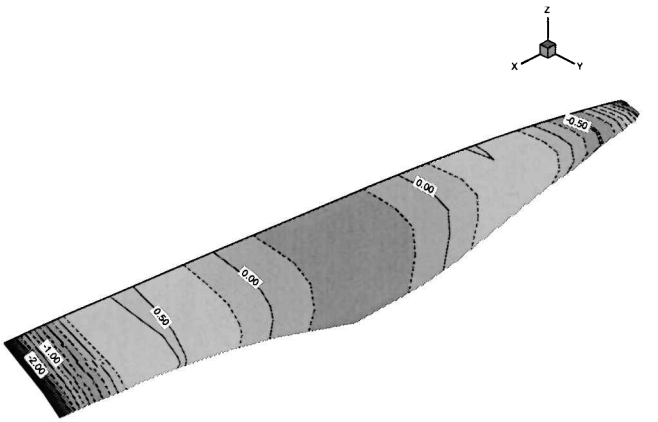

Fuselage

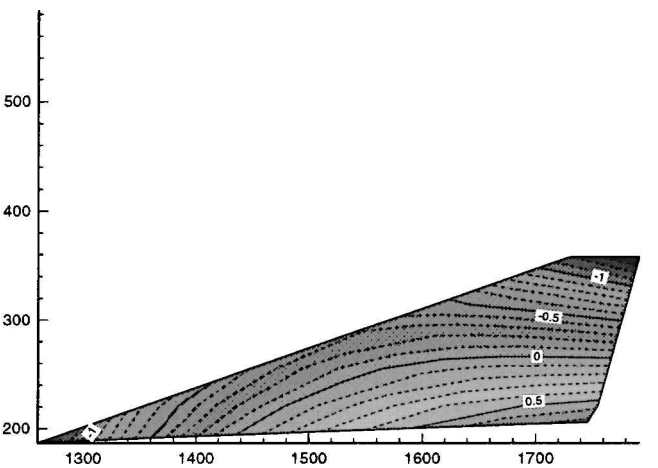

Wing

Fig. 12 Generic hypersonic vehicle mode 7 contours for the structural grid.

The remaining methods were excluded because of earlier discussed limitations for this particular configuration.

From the statistical summary of the maximum deflections in Table 6, it appears that the methods provide equivalent results, with the exception of the IPS interpolation of the fuselage. The TPS method once again provided results within 1% of the original data. For the wing, the MQ and IPS schemes yielded results within 5 and 6%, respectively. Both the scaled and unscaled results for MQ and TPS appear to provide equal results from this configuration. However, a comparison of the interpolated contours in Figs. 13–15 yield a different picture.

Figure 13 shows that IPS introduces some oscillations into the results of both the fuselage and wing. These oscillations change the location of the contour lines up to values of 10–15% of the fuselage cross section for mode 1 (not shown), but increase to 30–50% for the more complex mode 7 shown in Fig. 13. Similar, but less severe, oscillations can be seen on the wing, with errors in position of less than 2% of the span for mode 1 (not shown) and up to 100% for mode 7. Note that the implementation of the IPS method can be coded differently to yield better results for a particular geometrical

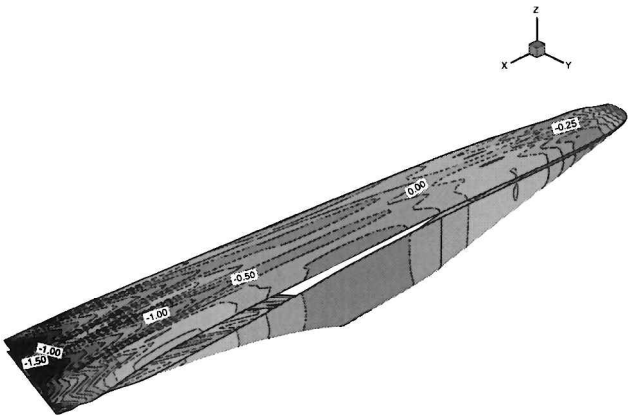

Fuselage contours

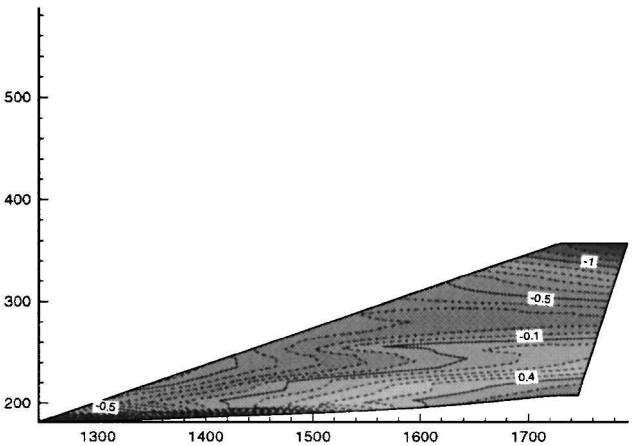

Wing contours

Fig. 13 Interpolation of generic hypersonic model mode 7 by IPS method.

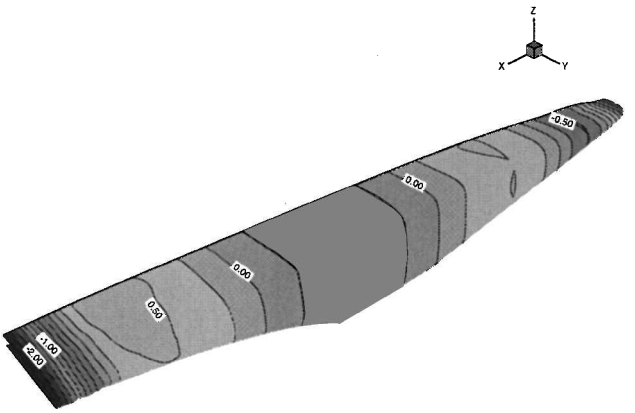

Fuselage contours

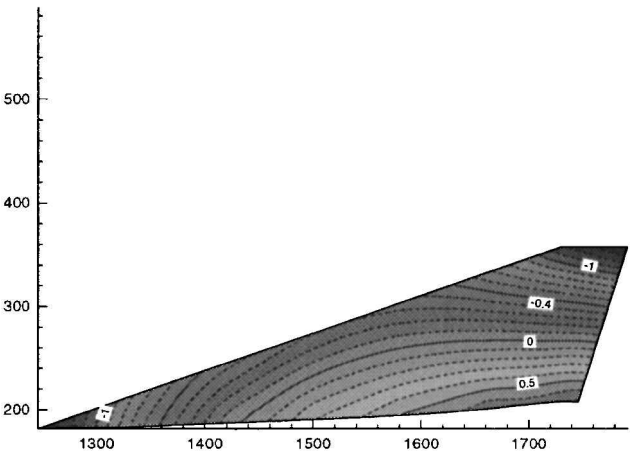

Wing contours

Fig. 14 Interpolation of generic hypersonic model mode 7 by MQ without scaling.

configuration. This implies that a user may have to modify the routine to obtain the optimum results for different types of geometries.

Figures 14 and 15 show that the MQ and TPS methods give excellent results if they are scaled. However, they do encounter problems on the fuselage interpolation if they are not scaled. Recall that the engine liner required that the MQ and TPS methods be scaled to provide reasonable results. Here, the numerical summary (as shown in Table 5) does not indicate a problem; however, plots of the interpolation do reveal moderate to severe oscillations, similar to those seen in Fig. 13 for the IPS interpolation.

F-16 Wing and Strake

The next example extends the capabilities demonstrated by the first three test cases. This example examines the extrapolation characteristics of each of the interpolation methods and examines their capabilities to handle discontinuities introduced by a control surface. The structural model is a flat plate that models an F-16 wing and comprises irregularly spaced nodes, as seen in Fig. 16a. The aerodynamic grid, shown in Fig. 16b, is a three-dimensional wing with the addition of a strake forward of the leading edge. Extrapolation is required for the strake region, as well as the leading and trailing edges of the wing. The strake extrapolation is a very exacting example of a fluid–structure interface problem.

The flat plate structural model for the wing has 24 nodes in the streamwise direction and 17 nodes along the spanwise direction. The aerodynamic model has 118 nodes along the streamwise direction (60 nodes for the upper and lower surfaces each) and 42 nodes along spanwise direction. This aerodynamic wing is constructed differently than the earlier examples. Here, the example is taken from an overset grid. The streamwise direction curves along the edge of the strake and around the wing leading edge and tip. Thus, the nodes are very highly clustered in the region of the strake edge and, although maintaining C^1 continuity, do change Cartesian coordinate directions dramatically.

The structural model consists of seven modes to model the shape of the wing, the seventh of which is shown in Fig. 17. The wing contours are modeled as shown in Fig. 17a, whereas the deflections are modeled as shown in Fig. 17b. Scaling is provided so that the results of the interpolations/extrapolations can be directly compared by overlaying the plots. For the deflections in Fig. 17b, the outline of the undeflected aerodynamic wing/strake is provided to show the large extent of extrapolation that is necessary. Notice that there is a control surface modeled as part of the wing. The control surface deflections include very abrupt changes in the mode in both directions (streamwise and spanwise) along the wing. These changes are especially noticeable in mode 7.

The IPS interpolation/extrapolation yields some interesting results, as demonstrated in Fig. 18 for mode 7. For modes 1 and 2, IPS does an excellent job of interpolation. At the higher modes where the motion of the control surface is evident, IPS has problems performing an accurate global interpolation. The deflections associated with the control surface deflection are captured within 5% (location and magnitude) of the original data in the spanwise direction. The IPS method shifts the location of the control surface edge from 67 to 73% of the span, as seen by the shift in the rapidly changing contours in that location. The modes in the chordwise direction are not predicted well at all. The peak seen at the outboard station on the input data (Fig. 17b) is not captured at all, but is lost in the smoothing action. This is also readily observed by comparison of the mode contours in Figs. 17a and 18a. The concentration of the rapidly changing contours inboard also shifts the interpolation of the modes aft, as seen by the average 70% aft shift of the zero contour line. The character of the zero contour line has also been modified in the chordwise direction. The extrapolation of the strake tends to

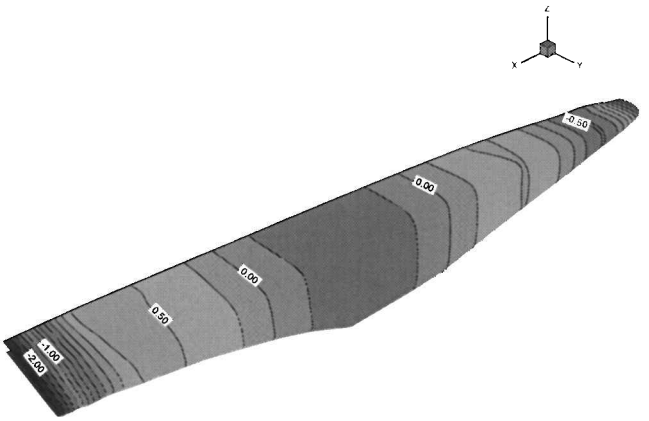

Fuselage contours

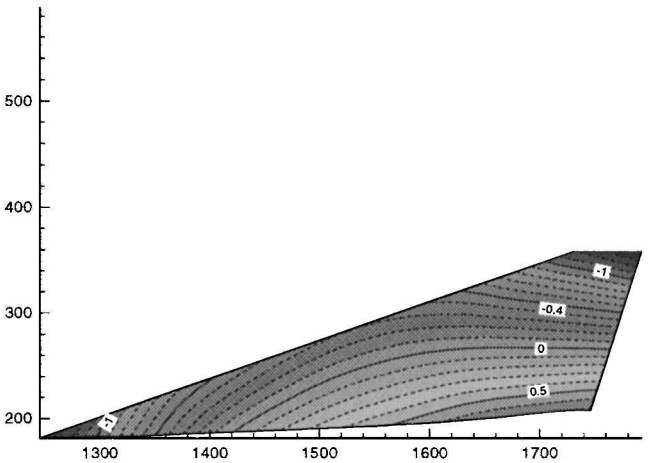

Wing contours

Fig. 15 Interpolation of generic hypersonic model mode 7 by thin plate method without scaling.

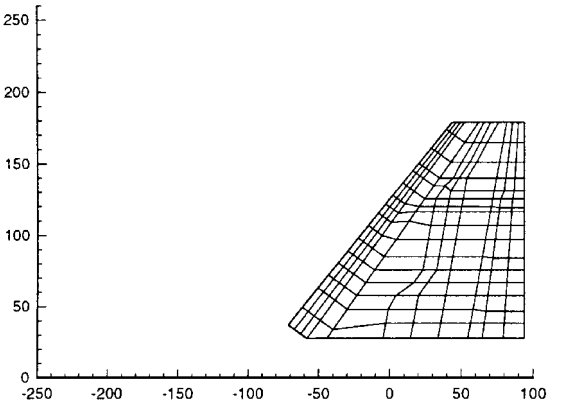

a) Structural grid

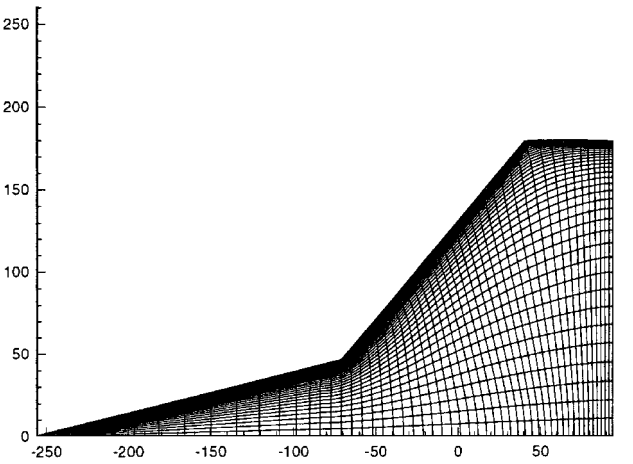

b) Aerodynamic grid

Fig. 16 F-16 wing/strake configuration.

be regular. The IPS method seems to extrapolate the contours linearly toward the root, based on the contours directly outboard. The control surface shape is continued to the root and is shifted forward, directly proportional to the changing span chord of the strake.

The MQ interpolation/extrapolation results for mode 7 are shown in Fig. 19. For all of the modes, the MQ interpolation method does not reach the full amplitude of the mode, but loses from 2 to 20% of the maximum value, depending on the rapidity of the changing mode. The MQ method has a tendency in this application to spread or distort the modes from 2 to 5% of the local span, as seen by comparing the contours in Figs. 17a and 19a. Because of this shift, large amplitudes near the edges are underpredicted up to 20%, and the area over which they act is also reduced. Because this phenomenon did not occur for the earlier, pure interpolation results, this spread could be the result of introducing the large extrapolation area of the strake. Extrapolation onto the strake takes two forms, depending on the orientation of the mode. For modes that end almost perpendicular to the structural wing root, the mode contour is extended almost to the strake root before turning to form a hill when it reaches the root. For mode contours that lie in a near-parallel orientation to the root, MQ causes no deflection of the strake. That is, a near-parallel zero contour adjacent to the strake is interpolated as zero deflection on the strake.

The TPS interpolation/extrapolation result is shown in Fig. 20. As in the MQ results, the contours are shifted slightly forward by 2–5% near the strake. The TPS interpolation also falls short of capturing the full mode amplitude, though at values approximately one-half the errors observed for the MQ interpolations. As in the MQ and TPS interpolations, the edge of the control surface has been shifted outboard, here less than 4%. Inboard of the wing, the contours perpendicular to the wing edge are extrapolated in a manner similar to

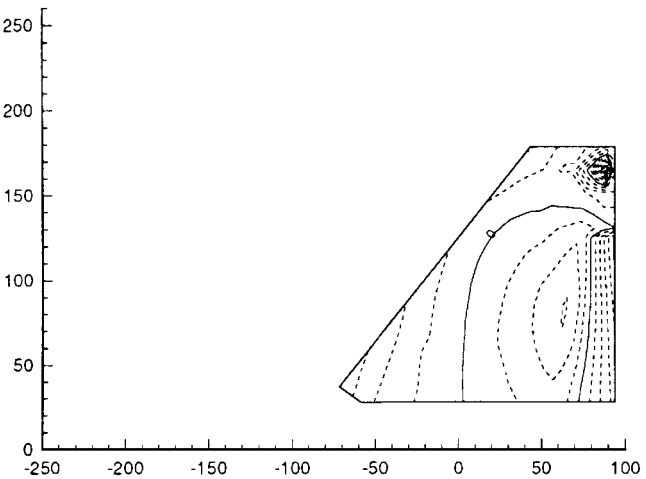

a) Mode contours

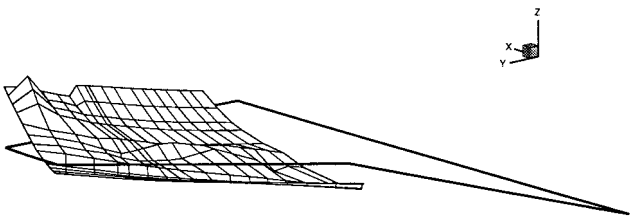

b) Mode deflections

Fig. 17 F-16 wing mode 7.

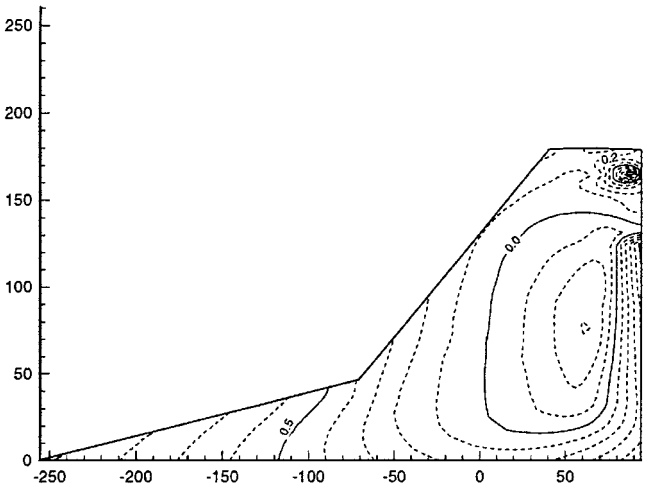

a) Mode contours

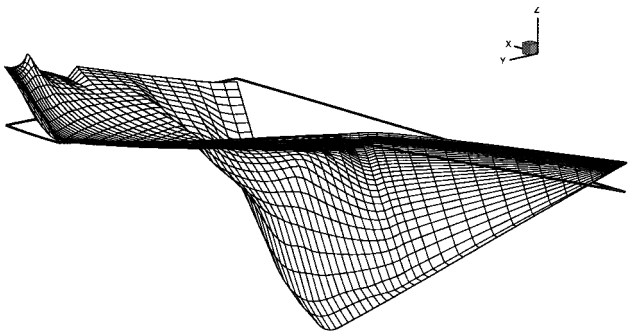

b) Mode deflections

Fig. 18 F-16 wing and strake mode 7 interpolations using the IPS method.

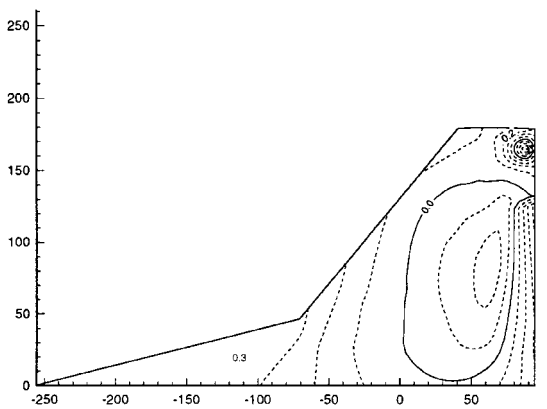

a) Mode contours

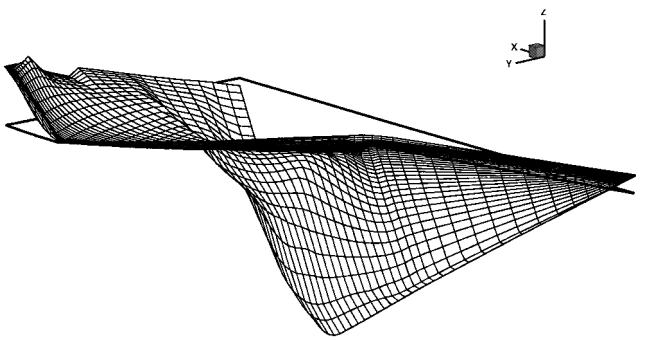

b) Mode deflections

Fig. 19 F-16 wing and strake mode 7 interpolations using the MQ method.

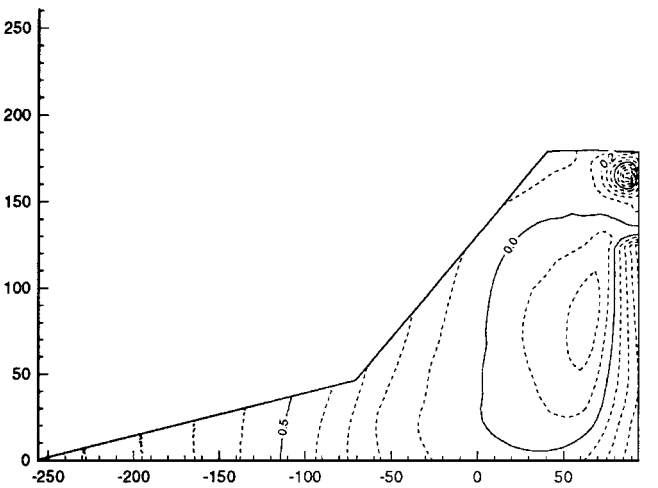

Mode contours

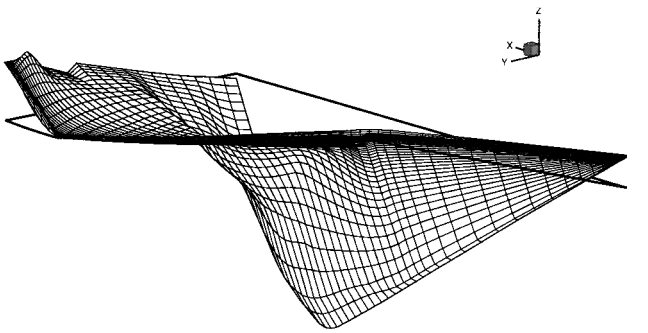

Mode deflections

Fig. 20 F-16 wing and strake mode 7 interpolations using the TPS method.

that noted for the MQ method. However, unlike the MQ method, the modes are interpolated linearly forward onto the strake. This is similar to the IPS method (as expected), but the contours remain more closely aligned with the axis system, rather than following the shape of the strake (Fig. 18a).

From these results, the characteristics of each of the methods in extrapolation can be seen. In the case of actual application of the F-16 wing/strake combination, the root would be cantilevered to the fuselage, forcing a zero deflection along the root chord. Thus, it would no longer serve as an extrapolation problem, as shown here, but would remain an exercise in interpolation.

F-16 Flexible Wing with Rigid Body

This test case involves an F-16 flexible wing attached to a rigid body. Unlike all of the preceding test cases, the wing structure is predicted using influence coefficients[23] rather than modes. In addition, this applications case is also used to examine the capability of the interpolation routines to integrate loads from the CFD wing to the structural node points.

The structure of the wing is predicted by 28 influence coefficients located at 7 nodes in the spanwise direction and 4 nodes in the streamwise direction, as shown in Fig. 21a. The wing is predicted as a flat plate surface, that is, the influence coefficients are taken to act normal to the direction of the undeflected structural surface.

The aerodynamic grid used in this test case is shown in Fig. 21b. The aerodynamic grid has 107 points wrapped from upper trailing edge to lower trailing edge, with 53 points on each surface. There are 25 nodes that determine the shape of the spanwise surface grid.

One set of influence coefficients is presented here. They are shown as contours for the structural grid in Fig. 22a. The F-16 flexible wing was examined without including its rigid fuselage in the configuration because there was no structural information for the fuselage.

The F-16 load computation was performed using integration of the pressures from the aerodynamic grid to the structural grid. The

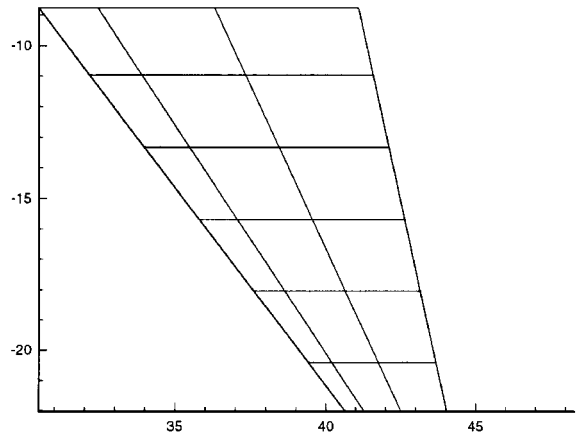

a) Structural mesh

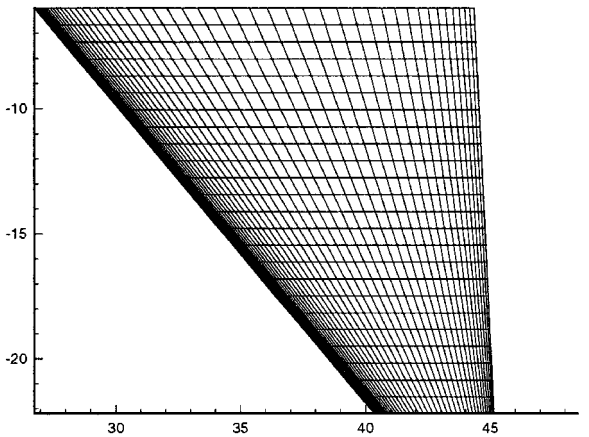

b) Aerodynamic surface grid

Fig. 21 F-16 wing configuration.

problem of transforming concentrated loads from one mesh to another can be based on the criterion of conservation of virtual work done by a set of applied loads. If F_a represents a column matrix of given concentrated loads at a set of points P_a, the virtual work done by this set of loads is given by

$$\delta W = F_s^T \delta u_a \tag{5}$$

where δu_a is compatible virtual discretized displacement field corresponding to the set of points P_a.

Consider now a second set of points P_s, not necessarily coincident with the first one. It is possible to define an equivalent set of concentrated loads on this second set such that the virtual work is the same. This condition will guarantee the preservation of total force and moment about any point on the system. If F_s is the set of concentrated forces on the set of points P_s that is equivalent to F_a, then

$$F_s^T \delta u_s = F_a^T \delta u_a \tag{6}$$

where δu_s is a compatible virtual discretized displacement field corresponding to the set of points P_s. To interpolate the displacement field between the two set of points,

$$u_s = T u_a \tag{7}$$

where T is the transformation matrix relating the two displacement sets. Because the virtual displacement fields have to be compatible, they also have to follow the same transformation. Therefore,

$$\delta u_s = T \delta u_a \tag{8}$$

Using this relation in the expression of the equivalence of virtual work, one gets

$$F_s^T T \delta u_a = F_a^T \delta u_a \tag{9}$$

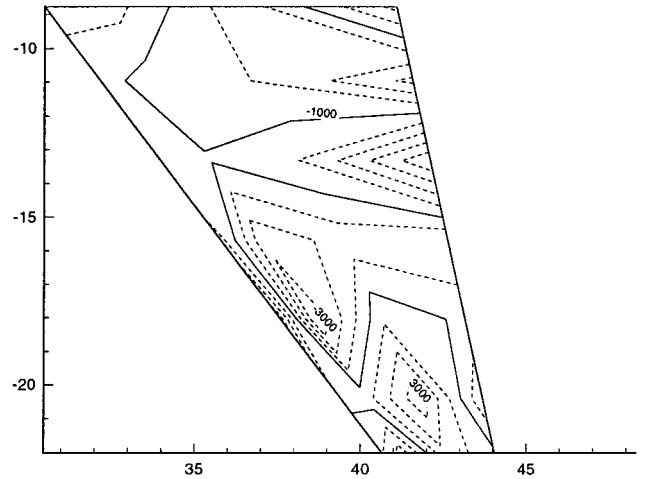

a) Structural influence coefficients

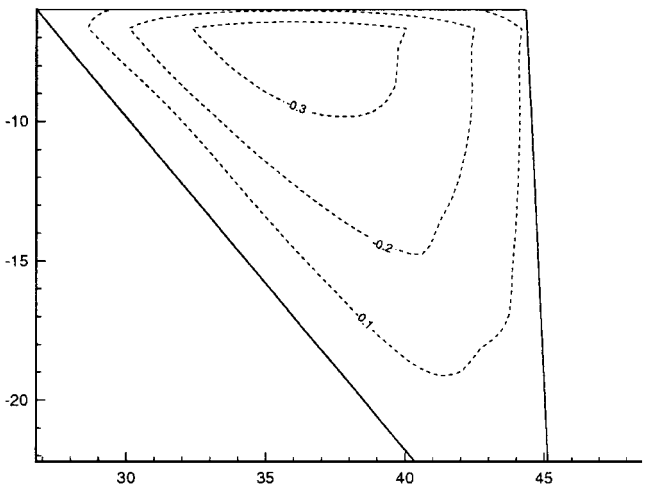

b) Wing pressures

Fig. 22 F-16 wing data used for load calculation and interpolation.

and

$$F_s^T T = F_a^T \tag{10}$$

Finally, the relation between the two sets of forces satisfying conservation of total force and moment is given by

$$F_a = T^T F_s \tag{11}$$

In standard finite element formulation, there is the problem of concentrated loads not applied at nodes. A way to handle the problem is by interpolating those loads to certain nodal points by means of a consistent nodal load transformation. This is basically the method described earlier. To put that within the finite element context, let us consider the matrix N as being the matrix of shape functions (local interpolation functions for the displacement within an element). Following directly from the general procedure outlined before, if Q is the concentrated force at a point P within an element that is not one of its nodes, then

$$F_a = N^T|_p Q \tag{12}$$

with F_n being the equivalent transformed nodal loads.

The F-16 flexible wing was examined independently of its rigid body. There was no structural information for the body. The influence coefficient interpolations are shown in Fig. 23 for the IPS, MQ, and TPS methods, respectively. It is relatively evident from the comparison of Figs. 22 and 23 that it is difficult to ascertain the accuracy of the interpolation of influence coefficients because of the sparseness of the input data. The MQ and TPS methods have a tendency

Table 7 Comparison of forces and moment errors associated with integration/interpolation of loads on F-16 Validation of Aeroelastic Tailoring (VAT) wing

Method	F_x	F_y	F_z	M_x	M_y	M_z
MQ (scaled)	0	2.9×10^{-14}	1.2×10^{-13}	100.0	4.1	1.2×10^{-13}
MQ (unscaled)	2.3×10^{-13}	1.9×10^{-14}	0	100.0	4.1	2.1×10^{-13}
TPS (scaled)	2.9×10^{-14}	0.0	3.3×10^{-14}	101.7	2.4	3.5
TPS (unscaled)	3.9×10^{-14}	0.0	3.3×10^{-14}	101.7	2.4	3.5

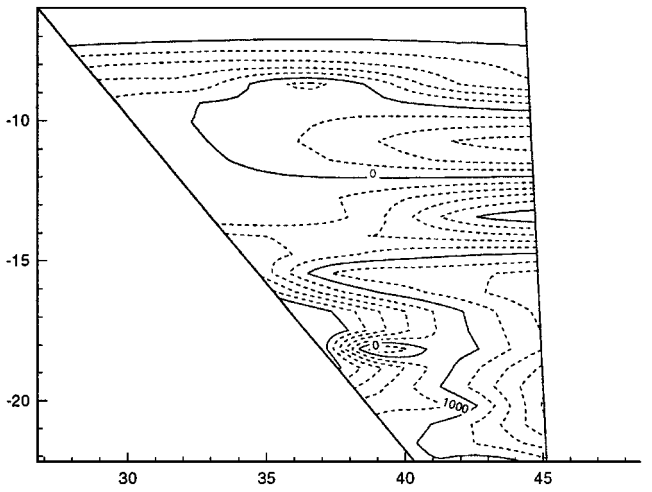

IPS method

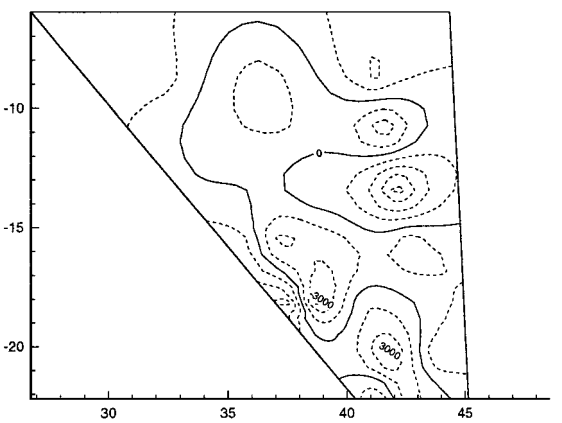

MQ method

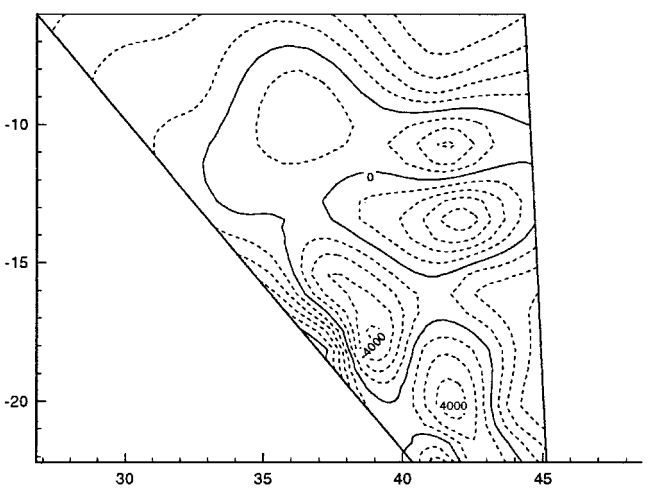

TPS Method

Fig. 23 F-16 wing structural influence coefficient interpolation.

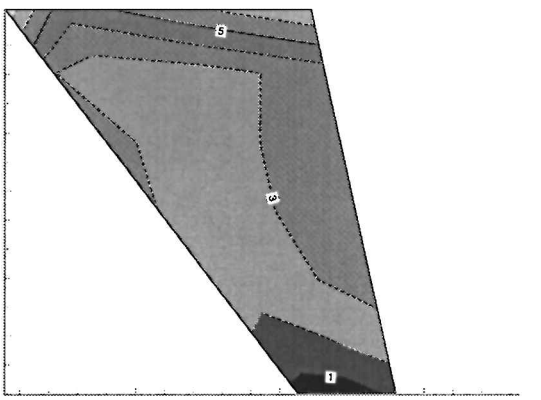

MQ method

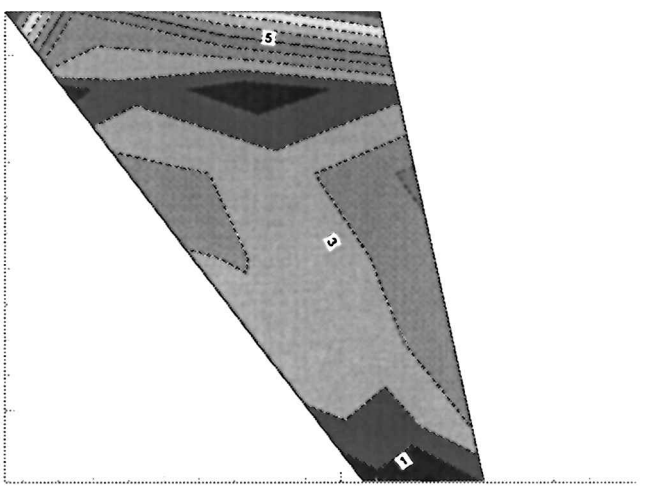

TPS method

Fig. 24 F-16 wing loads integration.

to smooth the sharp contours, but the relative pattern of peaks and valleys appear to be more accurately captured with these methods, particularly the MQ method. The TPS method tends to overshoot the values, sometimes as much as 25%, compared to the peak differences of 10% or less for the MQ method. In most applications, this computation is not done; instead the loads are computed and transferred to the structural grid.

The F-16 load computation was performed using integration of the pressures from the aerodynamic grid to the structural grid, as described earlier. These load computations are shown in Fig. 24 for MQ and TPS. There is no structural equivalent with which to compare these data. Instead, the forces and moments for the equivalent interpolated loads are integrated and compared with the integration of the original aerodynamic loads. These data are compared in Table 7. There are large excursions (errors) associated with the moment about the x axis (streamwise). This is because the data evaluated had little to no moment with respect to this axis for the flat plate (configuration interpolated to). The axes of interest are the y and z axes that were comparable in both configurations. The force errors for all variations of both schemes resided at machine zero.

For the moment errors, it appears that the MQ scheme performs better than the TPS scheme, with an essentially zero error in the normal moment (Mz) and a 4% error about the spanwise axis. The TPS scheme has a lower (2%) error about the spanwise axis but encounters a 3.5% error about the normal (most significant) axis. The overall errors (rms) for both schemes is approximately equal. When the contours in Fig. 24 are compared, there are some significant differences. The impact of these differences can only be assessed through the actual static aeroelastic solution of each method via comparison with experimental data.

Conclusions

A number of interpolation methods have been examined on a series of actual application test cases for Euler/Navier–Stokes-based aeroelastic tools. These interpolation methods included IPS, MQ, TPS, and NUBS. The accuracy and smoothness of the interpolations and extrapolations by each method was examined when interpolating mode shapes from the structural model to the aerodynamic model for various types of configurations currently being researched using nonlinear aerodynamic methods. In addition, the integration and interpolation of structural loads from the aerodynamic to the structural grid was examined for one case.

Based on the results presented here, along with those observed and reported in Ref. 15, several recommendations can be made for engineers who wish to perform CFD–CSD information transfer. First, several options should be available to the user because no one method provided the most accurate interpolation/extrapolation in all of the test cases. The most robust and accurate candidates are the MQ and the TPS methods. These schemes, with only minor exceptions for the MQ scheme, provided the most accurate and smooth data interpolation (within 5% of the initial magnitude and location). These two schemes also provided the most accurate data extrapolation of all of the methods. The MQ method does have some different extrapolation characteristics compared with the TPS method. Depending on the characteristics of the extrapolation desired by the user, either of these methods can be said to work equally well. All methods did encounter some accuracy difficulties when an attempt was made to interpolate data with sharp discontinuities, such as those encountered in mode shapes for a control surface/wing combination. The methods have a tendency to shift the discontinuity outboard by up to 5%, but the MQ and TPS methods do maintain the crispness of the discontinuity. These two methods, MQ and TPS, by their mathematical formulation, are also well suited to transfer finite element data encountered in lower-order CFD–CSD methods and also to handle unstructured grids.

Further research is recommended to quantify the impact of the interpolation and extrapolation errors on actual static and aeroelastic computations. Whereas the MQ and TPS methods provided the most accurate representation of the initial data, the errors encountered using the other methods may be offset by multiple modes (cancellation of errors in opposite directions). In particular, no quantitative conclusion can be drawn concerning the load integration until actual aeroelastic computations are performed and compared with experimental results.

Acknowledgments

The U.S. Air Force Research Laboratory Aeromechanics Division funded this research via Contract F33615-94-C-3010, Task 001. Kenneth Moran was the technical monitor, and the authors gratefully acknowledge the guidance he provided. The authors would like to thank Larry Huttsell of the U.S. Air Force Research Laboratory Aeroelasticity Branch for help in obtaining the data for many of these test cases, and for his technical discussions pertaining to their utilization. The authors would like to acknowledge the technical expertise provided on algorithms developed or coded by Richard Franke of Naval Postgraduate School, Kari Appa of Northrop Corporation, Robert Ames of David Taylor Research Center, and Robert Fithen of the University of New Orleans.

References

[1]Guruswamy, G. P., and Byun, C., "Fluid-Structural Interactions Using Navier–Stokes Flow Equations Coupled with Shell Finite Element Structures," AIAA Paper 93-3087, July 1993.

[2]Schuster, D. M., Vadyak, J., and Atta, E., "Flight Loads Prediction Methods for Fighter Aircraft," Wright Research and Development Center-TR-89-3104, Nov. 1989.

[3]Byun, C., and Guruswamy, G. P., "A Comparative Study of Serial and Parallel Aeroelastic Computations of Wings," NASA TM 108805, Jan. 1994.

[4]Robinson, B. A., Batina, J. T., and Yang, H. T. Y., "Aeroelastic Analysis of Wings Using the Euler Equations with a Deforming Mesh," *Journal of Aircraft*, Vol. 28, No. 11, 1991, pp. 781–788.

[5]Smith, M. J., Huttsell, L., Schuster, D. M., and Buxton, B., "Development of an Euler/Navier–Stokes Aeroelastic Method for Three-Dimensional Vehicles with Multiple Flexible Surfaces," AIAA Paper 96-1513, April 1996.

[6]Smith, M. J., "Computational Considerations of an Euler/Navier–Stokes Aeroelastic Method for a Hovering Rotor," *Journal of Aircraft*, Vol. 33, No. 2, 1996, pp. 429–434.

[7]Done, G. T. S., "Interpolation of Mode Shapes: A Matrix Using Two-Way Spline Curves," *Aeronautical Quarterly*, Vol. 16, Pt. 4, Nov. 1965, pp. 333–349.

[8]Conte, S. D., and de Boor, C., *Elementary Numerical Analysis*, McGraw–Hill, New York, 1980, pp. 289–293.

[9]Harder, R. L., and Desmarais, R. N., "Interpolation Using Surface Splines," *AIAA Journal*, Vol. 9, No. 2, 1972, pp. 189–191.

[10]"Handbook for Aeroelastic Analysis," Vols. 1 and 2, MacNeal–Schwindler Corp., Nov. 1987.

[11]Johnson, E. H., and Venkayya, V. B., "Automated Structural Optimization System (ASTROS)," Vol. 1, AFWAL-TR-88-3028, Air Force Wright Aeronautical Labs., Wright–Patterson AFB, OH, Dec. 1988.

[12]Shan, R., "MPROC3D: User and Program Reference Guide," U.S. Air Force Research Lab./Aeroelasticity Branch Contract F33657-90-D-2189, Task 012, Oct. 1993.

[13]Blair, M., "Unified Aeroelastic Surface Formulation," AIAA Paper 94-1471, April 1994.

[14]Franke, R., "Scattered Data Interpolation: Tests of Some Methods," *Mathematics of Computations*, Vol. 38, No. 157, 1982, pp. 181–200.

[15]Smith, M. J., Hodges, D. H., and Cesnik, C. E. S., "An Evaluation Of Computational Algorithms to Interface Between CFD And CSD Methodologies," U.S. Air Force Research Lab., TR-96-3055, Nov. 1995.

[16]Hardy, R. L., "Multiquadric Equations of Topography and Other Irregular Surfaces," *Journal of Geophysical Research*, Vol. 76, No. 8, 1971, pp. 1905–1915.

[17]Kansa, E. J., "Multiquadrics—A Scattered Data Approximation Scheme with Applications to Computational Fluid Dynamics, Parts I and II," *Computers and Mathematics with Applications*, Vol. 19, No. 8/9, 1990, pp. 127–161.

[18]Duchon, J., "Splines Minimizing Rotation-Invariant Semi-Norms in Sobolev Spaces," *Constructive Theory of Functions of Several Variables, Oberwolfach 1976*, edited by W. Schempp and K. Zeller, Springer–Verlag, Berlin, 1977, pp. 85–100.

[19]*DT_NURBS Spline Geometry Subprogram Library User's Manual*, Boeing Computer Services, Ver. 2.3, Feb. 1995, pp. 3-1–4-5.

[20]Yates, E. C., "AGARD Standard Aeroelastic Configurations for Dynamic Response, I. Wing 445.6," AGARD-R-765, 1985.

[21]Ziada, S., Buhlmann, E. T., and Bolleter, U., "Model Tests on Shell Flutter Due to Flow on Both Sides," *Journal of Fluids and Structures*, Vol. 2, 1988, pp. 177–196.

[22]Rickets, R. H., Noll, T. E., Whitlow, W., and Huttsell, L. J., "An Overview of Aeroelasticity Studies for the National Aero-Space Plane," AIAA Paper 93-1313, April 1993.

[23]Roger, W. A., Brayman, W. W., Murphy, A. C., Graham D. H., and Love, M. H., "Validation of Aeroelastic Tailoring by Static Aeroelastic and Flutter Tests," AFWAL-TR-81-3160, Air Force Wright Aeronautical Labs., Wright–Patterson AFB, OH, Sept. 1982.